Statistical uncertainty of 2.5×10^{-16} for the ^{199}Hg $^1S_0 - ^3P_0$ clock transition against a primary frequency standard

J. J. McFerran,[1,2] L. Yi,[1] S. Mejri,[1] W. Zhang,[1] S. Di Manno,[1] M. Abgrall,[1] J. Guéna,[1] Y. Le Coq,[1] and S. Bize[1,*]

[1]*Laboratoire National de Métrologie et d'Essais - Systèmes de Référence Temps-Espace (LNE-SYRTE), Observatoire de Paris, CNRS, UPMC, 61 Avenue de l'Observatoire, 75014 Paris, France*

[2]*School of Physics, M013, The University of Western Australia, Crawley, 6009, Western Australia, Australia*

(Received 11 March 2014; published 30 April 2014)

High-resolution spectroscopy has been carried out on the ^{199}Hg $^1S_0 - ^3P_0$ spin and dipole forbidden transition, where the atoms are confined in a vertical one-dimensional optical lattice trap using light at the magic wavelength. We describe various characteristics of the resulting line spectra and assess the strength of the Lamb-Dicke confinement. Through a series of absolute frequency measurements of the ^{199}Hg clock transition with respect to the LNE-SYRTE primary frequency standard, recorded over a 3-month period, we demonstrate a statistical fractional uncertainty of 2.5×10^{-16}. We include details relating to the generation of ultraviolet light at three wavelengths necessary for the experiment: 253.7 nm for cooling and detection, 265.6 nm for clock transition probing, and 362.570 nm for lattice trapping, along with further aspects related to the magic wavelength evaluation.

DOI: 10.1103/PhysRevA.89.043432 PACS number(s): 32.30.Jc, 37.10.Jk, 42.62.Fi, 37.10.De

I. INTRODUCTION

The development of highly accurate frequency references is an active field of study motivated, in large part, by the aim to develop secondary frequency standards representing the SI second and, ultimately, to establish a new definition for the SI second [1,2]. Tests of fundamental physics also drive their development; for example, atomic frequency references have been used to search for tenable temporal changes in fundamental constants [3–5]. As their accuracy has improved, tighter constraints have been placed on the drift rate of the electron-to-proton mass ratio [6,7] and the fine-structure constant [5,7,8]. The measurement of frequency ratios between clock transitions of different atomic species also provides a sensitive test of the gravitational redshift when looking for annual changes as the gravitational potential varies [6–8]. The sensitivity of these tests is expected to improve as frequency-stabilized optical fiber networks extend in coverage [9–12] and more accurate clocks with dedicated communication links are placed in orbit, allowing clock-to-clock comparisons across the globe [13,14]. Along with tests of fundamental physics, a wide network of clock-frequency comparisons should produce more precise geodesy measurements through the gravitational redshift [14,15], providing useful geophysical information related to hydrological flows and subsurface density anomalies [16,17].

A contender for a future 10^{-18} accuracy range clock is one based on neutral ^{199}Hg atoms constrained in an optical lattice trap [18]. Recently, the frequency of the ^{199}Hg $^1S_0 - ^3P_0$ clock transition was measured with a fractional accuracy of 5.7×10^{-15} [19] and fractional frequency instability of $5.4 \times 10^{-15}/\sqrt{\tau}$ ($2 < \tau \lesssim 400$ s) [20]. Mercury is favorable as a frequency reference for several reasons. First, its sensitivity to blackbody radiation is less than one-tenth that of more well-established lattice clocks [18], namely, Yb and Sr, where the contribution to uncertainty budgets have been dominated by this systematic shift [21–24]. Second, Hg has an exceedingly high vapor pressure at room temperature; hence a high-temperature oven is not required, which can otherwise make assessment of the temperature of surrounding surfaces more complicated (thus affecting the uncertainty of the blackbody shift). Third, one of the naturally occurring isotopes of mercury (^{199}Hg) has a nuclear spin of $\frac{1}{2}$; hence the dual magnetic sublevels simplify optical pumping for spin polarization; moreover, there are no tensorial lattice shifts for the spin-$\frac{1}{2}$ system (as with ^{171}Yb).

Sub-10^{-15} statistical uncertainty has been demonstrated on several occasions between microwave transitions, for example, between Cs primary frequency standards (PFSs) [25,26] and between Rb and Cs [7]. Also, sub-10^{-16} statistical uncertainty was demonstrated for the Al^+-Hg^+ comparison, which avoided any intermediary primary frequency standard [5]. However, repeated measurements between an optical transition frequency and a primary frequency standard over the course of months at the sub-10^{-15} level is uncommon. Recently, measurements of the ^{87}Sr $^1S_0 - ^3P_0$ transition against a PFS has demonstrated a statistical variation of 3.1×10^{-16} [27].

A statistical uncertainty lower than the total systematic uncertainty provides some confirmation that the systematic uncertainties have not been underestimated. We demonstrate here frequency measurements of the ^{199}Hg clock transition with one of the lowest statistical uncertainties for an optical frequency transition regularly measured over several months: $\Delta\nu_{\mathrm{stat}} = 2.5 \times 10^{-16}$. We note that accuracy limitations produced by even the best PFSs can be avoided by comparing clocks solely in the optical domain [28,29], but for the present time the Cs PFS needs to be used to test the reproducibility of clocks.

In this article we provide greater details of the procedures used to generate the results presented in Ref. [19] and highlight the low statistical uncertainty achieved with $^1S_0 - ^3P_0$ transition (Ref. [19] focuses on the systematic uncertainty). To detail the LNE-SYRTE ^{199}Hg clock experiment we organize the paper as follows. Section II describes the parts of the experiment, providing, in particular, details about the five resonant frequency-doubling stages needed for producing

*sebastien.bize@obspm.fr

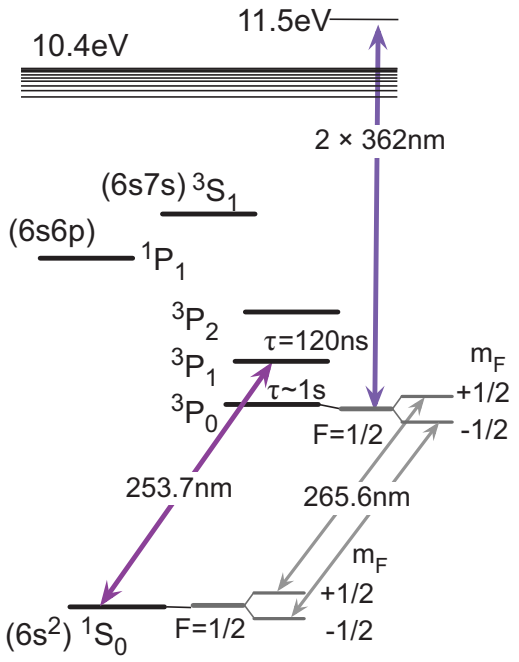

FIG. 1. (Color online) Relevant energy levels for ^{199}Hg. The transitions highlighted correspond to laser cooling (253.7 nm), lattice trapping (362.5 nm), and clock transition probing (265.6 nm).

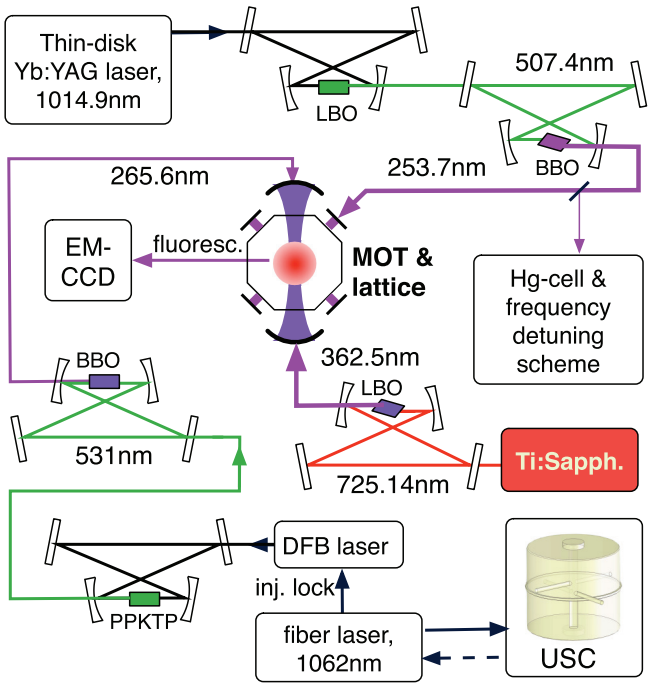

FIG. 2. (Color online) The main experimental components for producing the magneto-optical trap (MOT), lattice trap, and ^{199}Hg spectroscopy. USC, ultrastable cavity; DFB, distributed feedback laser diode; crystals: BBO, beta barium borate; LBO, lithium triborate; PPKTP, periodically poled potassium titanyl phosphate. Mode-matching optics and mirrors are omitted for clarity.

three important wavelengths. Section III discusses various ^{199}Hg spectra, including motional sideband spectra from which the lattice depth is deduced. Section IV provides a broad account of lattice light shift measurements, and Sec. V details the means by which frequency measurements were taken and discusses the results.

II. EXPERIMENT

Up to now three laser wavelengths have been used to interact with the ^{199}Hg atoms. These are needed (i) to probe the clock transition (265.6 nm), (ii) to trap the atoms in a dipole lattice trap (362.6 nm), and (iii) to cool and detect the atoms (253.7 nm). The wavelengths are seen in the energy-level diagram of Fig. 1. The ultraviolet wavelengths used for cooling and probing are both generated through two resonant frequency-doubling stages, all with bow-tie cavity configurations, as summarized in Fig. 2. The source for the cooling light is a Yb-doped YAG thin-disk laser with its wavelength tuned to 1014.9 nm. The laser cavity length is 780 mm, and the radius of curvature of the disk is approximately 1.2 m, forming a spot size e^{-2} of 740 and 410 μm at the disk and output coupler, respectively. Up to 6 W can be generated by the disk laser, but we typically operate with ~3.5 W in order to prolong the lifetime of the disk. This light is mode matched to a resonant frequency-doubling cavity that contains a 15-mm-long, noncritically phase-matched ($\theta = 90°$, $\phi = 0°$) lithium triborate (LiB_3O_5) crystal for the frequency upconversion. Approximately 1.7 W is produced at 507.4 nm when the LiB_3O_5 crystal is maintained at the phase-matching temperature of ~210 °C. The second-stage frequency-doubling cavity uses a 7-mm-long, Brewster-cut, critically phase-matched (type I, $\theta = 51.4°$) beta barium borate (β-BaB_2O_4) crystal. The round-trip cavity length is 1.25 m and has a folding angle of $\alpha/2 = 9.5°$. The two focusing mirrors have a radius of curvature of 100 mm, forming a waist of 19 μm (31 μm) in the sagittal (tangential) plane at the center of the crystal. The β-BaB_2O_4 crystal is maintained at ~40 °C to minimize water-vapor deposition and has O_2 gas directed onto the exit face of the crystal (with a flow rate of $\sim 10^{-6}$ m^3 s^{-1}). A summary of the frequency-doubling cavity details is provided in Table I, where l_C is the crystal length, ρ is the walk-off angle, RoC is the radius of curvature of the focusing mirrors, ω_{0s} and ω_{0t} are the sagittal (vertical plane) and tangential (horizontal plane) waist sizes, and R_{ic} is the reflectivity of the input coupler for the fundamental light.

The clock probe light at 265.6 nm, with its much reduced demands on optical power, begins with a distributed feedback (DFB) laser that has its output frequency quadrupled through two resonant bow-tie cavities. There is 250 mW available for the quadrupling process. A continuous-wave Yb:fiber laser at 1062.6 nm locked to an ultrastable cavity, as described in Refs. [20,30,31], is split three ways via optical fiber links to (i) the main Hg apparatus, (ii) an Er:fiber-based frequency comb, and (iii) a Ti:sapphire-based frequency comb (further details below). The 1062.6-nm light sent to the Hg apparatus injection locks the DFB laser, with approximately 10 MHz of bandwidth, to confer a phase lock between the ultrastable laser and DFB light. The DFB needs to be maintained at −10 °C to reach the necessary frequency for injection locking. The first frequency-doubling stage producing 531.3-nm light contains a 20-mm-long periodically poled potassium titanyl phosphate

TABLE I. Summary of parameters for the frequency-doubling bow-tie cavities. PP, periodically poled. See text for other definitions.

λ_0 (nm)	Crystal	l_C (mm)	θ (deg)	ϕ (deg)	ρ (mrad)	RoC (mm)	$\alpha/2$ (deg)	ω_{0s}, ω_{0t} (μm)	R_{ic} (%)
1062.6	$KTiOPO_4$ (PP)	20			0	77.5	10.5	36, 37	92
1014.9	LiB_3O_5	15	90	0	0	75	8.5	35, 33	92
724.1	LiB_3O_5	15	90	40.7	18.5	100	13.6	32, 46	98.7
531.3	β-BaB_2O_4	7	47.7	90	85.3	100	9.4	29, 28	98.4
507.4	β-BaB_2O_4	7	51.4	90	84.8	100	9.4	19, 31	98.5

($KTiOPO_4$) crystal with a 92% reflectivity mirror as the input coupler and has a beam waist of 36 μm at the crystal.

The conversion efficiency is approximately 60%. The second doubling stage to 265.5 nm uses a 7-mm-long, critically phase-matched (type I, $\theta = 47.7^\circ$), antireflection-coated β-BaB_2O_4 crystal with a beam waist of 29 μm and uses a mirror with 98.4% reflectivity for the input coupling.

A broadly tunable Ti:sapphire laser is the source for the lattice light. The light is frequency doubled in a fifth bow-tie buildup cavity, this time employing the Hänsch-Couillaud locking scheme, and produces about 160 mW at 362.6 nm (early measurements produced as much as 240 mW). The nonlinear element is a 15-mm-long Brewster-cut LiB_3O_5 crystal with $\theta = 90^\circ$ and $\phi = 40.7^\circ$ (type I, critically phase matched with a walk-off of 18.5 mrad between the fundamental and the second-harmonic radiation). The radius of curvature of the focusing mirrors is 100 mm, and the folding angle is $\alpha/2 = 13.7^\circ$, producing an e^{-2} radius at the waist inside the crystal of 32 μm (46 μm) in the sagittal (tangential) plane. The cavity design is similar to that found in Ref. [32].

Figure 3 summarizes the operating sequence of the magneto-optical trap (MOT) fields, CCD camera, MOT displacement B field B_x, and the 265.6-nm probe beam. The lattice light remains on continuously throughout the cycle. A necessary aspect of the Hg experiment is to displace the MOT loaded atoms into the lattice light waist since manipulation of the lattice cavity is not straightforward. With the lattice beam vertical, displacement of the atoms only needs to be carried out in the horizontal plane, which is achieved using bias magnetic fields. We define the following directions: z is vertical, y is along the strong axis of the MOT, and x is orthogonal to y in the horizontal plane. In the y direction the atom cloud is displaced by shunting a small fraction of current from one of the two MOT coils, while in the x direction the displacement is carried out with an auxiliary field coil located close to the MOT. The x direction also acts as the quantization axis for the clock signal generation; hence it is important that this displacement field is extinguished for the clock transition probe (denoted B_x in Fig. 3). A larger coil is used to set the bias B field for the quantization axis, which remains at constant field strength (or vanishing field strength in the case where the Zeeman components of the clock transition overlap).

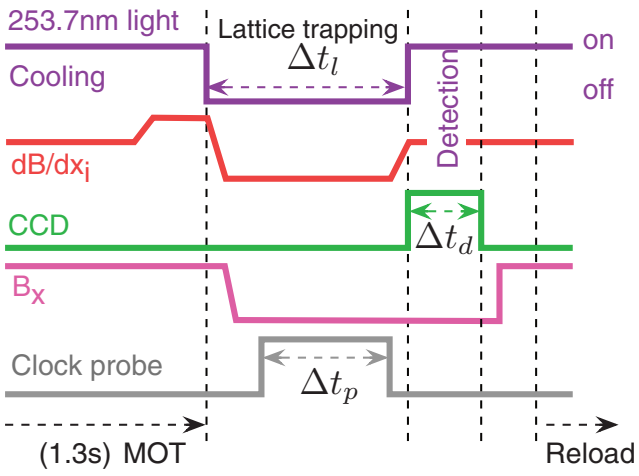

FIG. 3. (Color online) Operational sequence of the MOT fields, CCD camera, MOT displacement B field B_x, and the 265.6-nm probe beam. The lattice light remains on continuously throughout the cycle. $\Delta t_l = 80$ ms and $\Delta t_p = 50$ ms unless otherwise stated; $\Delta t_d = 9$ ms.

We find the optimum detection duration to be ~9 ms [33]. This could increase if intensity variations across the 253.7 nm beam profile were reduced (the shot-to-shot total-intensity variations are accounted for, but if the intensity varies across the beam profile, it creates the limiting detection level). Most of the spectroscopy so far has been carried out with $\Delta t_l = 80$ ms and $\Delta t_p = 50$ ms, as defined in Fig. 3 (previously, we showed that an atomic quality factor of 10^{14} can be achieved with $\Delta t_p = 80$ ms [19]). A present limitation to the probe duration is the lifetime of the atoms in the lattice, which we find to be ~250 ms (at e^{-1}). The scattering rate of lattice photons from the Hg atoms with 1.1 × 10^9 W m^{-2} of intensity (at 21 E_R) is about 4 × 10^{-14} s^{-1} [34]. Thus the recoil heating is negligible. Intensity noise considerations [35] predict a lifetime of several seconds [36]. Therefore it seems background gas collisions (mainly Hg) are likely to be contributing to the reduced lattice trap lifetime. We do have control of the background pressure (with a time constant of several hours) [33]; however, reducing the background vapor pressure slows down the loading of the MOT.

III. SPECTRA

In earlier stages of the experiment, spectral measurements of the clock transition showed full width at half maxima (FWHM) of a few kilohertz [37]. Important factors in reducing the linewidth have been (i) to increase the lattice trap depth to prevent tunneling between lattice sites [33], (ii) to have the lattice light as close to the magic wavelength as measurement uncertainty allows (now λ_m= 362.5697 ± 0.0011 nm), (iii) to limit the probe power so that it approaches a π Rabi area, and (iv) to carefully set bias magnetic fields. The increase in lattice depth was achieved by a slight change in cavity design. Mirrors with a radius of curvature of 250 mm are positioned above and below the MOT chamber (while sealing the vacuum chamber), enabling a trap depth up to ~25 E_R (or 9 μK). After

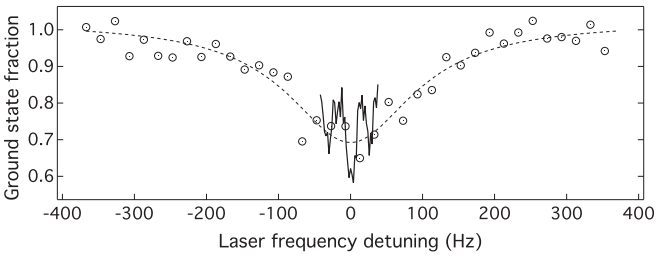

FIG. 4. Spectra of the ^{199}Hg clock transition recorded with frequency steps of 20 Hz (open circles) and 2 Hz (solid line). The FWHM of the broad (narrow) spectrum is 210 Hz (15 Hz). The same probe pulse length of 50 ms was applied in both cases.

implementing the above approaches, we have a clock transition that is a combination of an ultranarrow ∼10 Hz wide line centrally superimposed on a broader background profile, as illustrated in Fig. 4. The two traces in Fig. 4 were recorded in succession. From an ensemble of 36 measurements the mean linewidth of the background profile is $\Delta\nu_L = 149 \pm 24$ Hz. It would appear that a sizable proportion of atoms experiences some motional effects and is not fully confined to the Lamb-Dicke regime. A conceivable explanation for the broadened line is that of transit-time broadening arising from atoms escaping in the transverse directions and being probed for a duration shorter than that of the Rabi pulse. For example, if we consider a temperature just above the trap depth, e.g., ∼10 μK, then the mean distance traveled by an atom is 1.6 mm, which is wider than the beam diameter e^{-2} of 620 μm, suggesting that atoms that have escaped the trap are susceptible to transit-time effects. However, estimates of the linewidth associated with transit-time broadening appear to be too small to explain the observations. Comments about the distribution of atoms among the motional states appear below.

We see from Fig. 4 that if the atoms producing the background profile could participate in the formation of the ultranarrow line, then its contrast would increase dramatically. The expectation is that this will happen when the lattice trap is made deeper (or if more atoms are moved into the lowest vibrational state). A means of confining the atoms more tightly is to increase the focusing strength of the lattice light. For example, a twofold reduction of the waist size to 60 μm increases the lattice depth fourfold, making it approximately $100E_R$ (comparable to other Sr and Yb lattice clock experiments). Another means is to apply transverse cooling with the 265.6-nm light. Misalignment between probe and lattice beams was considered a possible reason for the background profile since misalignment renders the probe sensitive to the motion of the atoms in the transverse directions.

Deliberate misalignment of the lattice and probe beam was observed to destroy the ultranarrow feature, but it did not affect the broader background spectrum significantly. Despite the low contrast of the narrower clock signal, there is sufficient signal-to-noise ratio (SNR) to make reliable frequency measurements.

Figure 5(a) shows a clearer ^{199}Hg spectrum obtained with a 50-ms rectangular pulse and a probe intensity of ∼4×10^{-4} W cm^{-2} (with a predicted Rabi area of ∼5π rad). There are two fitted traces: the solid line shows a Lorentzian line shape with

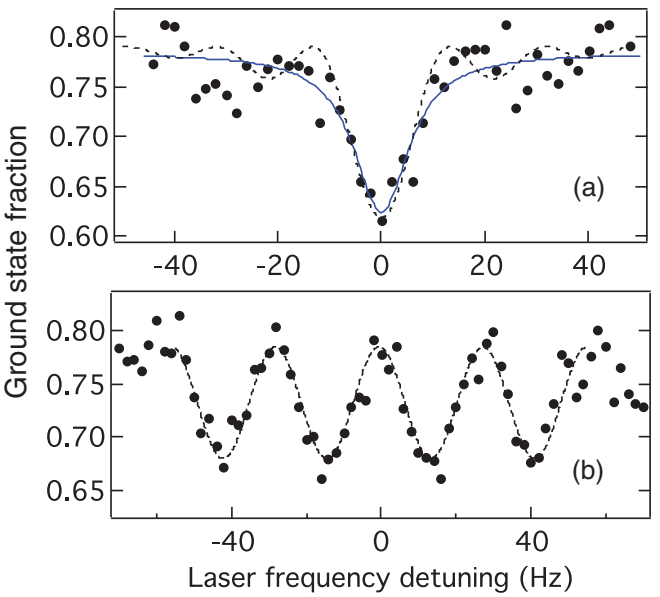

FIG. 5. (Color online) Ground-state fraction versus the probe laser's frequency detuning for: (a) a single 50-ms square pulse and (b) a pulse pair with 34-ms separation and a pulse duration of 6 ms.

a FWHM of 14 Hz, and the dashed line is the modeled Rabi spectrum with $\Omega T \sim 1.2\pi$ rad. The linewidth is consistent with the Fourier-transform-limited width expected from a 50-ms rectangular pulse (i.e., 16 Hz). There is a suggestion of sidebands at about 30 Hz from the carrier. Although it seems plausible that these sidebands are due to a slightly overdriven transition, we conclude that the sidebands most likely originate from technical noise since the offset from the carrier does not change with probe duration. If the sidebands corresponded to the transverse frequency of the lattice trap (with the probe not perfectly parallel to the lattice beam), the 30 to 35 Hz frequency offset would correspond to a lattice depth of only $11E_R$ (4 μK), about half of that determined from power estimates in the cavity and the analysis below. Figure 5(b) shows Ramsey fringes generated by use of a pulse pair with 34-ms separation and a pulse length of 6 ms. The sinusoidal fit has a period of 28 Hz, consistent with the inverse of the pulse separation time. $Q > 10^{13}$ spectra for the ^{199}Hg clock transition were in fact found first using the Ramsey pulse sequence.

Information about the confinement of the atoms in the lattice trap is obtained by examining the sideband spectra of the Lamb-Dicke spectrum. An example is shown in Fig. 6, where the intensity was increased by approximately 500 to enhance the sidebands. The carrier was recorded under normal probing conditions. We can apply a curve fit to the blue sideband using the approach outlined in [38,39], where, apart from vertical scaling, the only free parameters are the lattice depth U_0 and the temperature in the transverse direction T_r. The expression for the fit function in terms of the frequency detuning δ is

$$a(\delta) = A\left(1 - e^{-\frac{hf_r}{k_B T_r}}\right)^2 e^{-\frac{hf_r}{k_B T_r}} e^{-\frac{4U_0}{k_B T_r}\left(1-\frac{\delta}{f_z}\right)} \frac{4U_0}{hf_r}\left(1 - \frac{\delta}{f_z}\right), \quad (1)$$

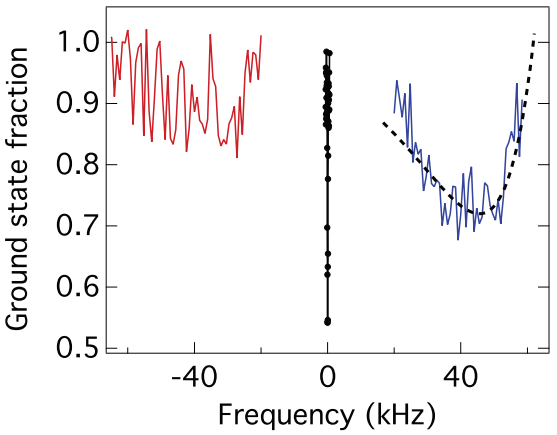

FIG. 6. (Color online) A sweep of the ^{199}Hg clock transition showing the red and blue motional sidebands on either side of the carrier. The transition is heavily saturated for the sidebands (but not the carrier). The line fit to the blue sideband is used to determine the trap depth and transverse temperature.

where f_z is the axial frequency, f_r is the transverse frequency, k_B is Boltzmann's constant, and h is Planck's constant (f_z and f_r are dependent upon U_0). We find $U_0 = 18E_R$ (or 6.5 μK) and $T_r = 6.3\,\mu$K, with associated axial and transverse frequencies of 62 kHz and 42 Hz, respectively. We estimate the temperature of the atoms in the axial direction based on the ratio of the blue and red sidebands to be ∼3.5 μK (with $P_n/P_{n+1} \sim 2.4$). With these values we determine the mean occupation numbers to be $\langle n_z\rangle = 0.8$ and $\langle n_x\rangle = \langle n_y\rangle \sim 3000$; thus transverse excited states are heavily populated, and these atoms are more likely to escape the trap. This lends support to the earlier mention that escaping atoms may be contributing to the background profile of Fig. 4.

IV. LATTICE LIGHT SHIFT

Most of the investigations related to the systematic uncertainty of the ^{199}Hg clock transition have, so far, been with respect to the first-order Stark shift produced by the lattice trapping light. Initial measurements were recorded with $\Delta\nu_L =$ 2–3 kHz line spectra, which produced a 0.21-nm (580-ppm) uncertainty for the magic wavelength [37].

Figure 7 shows the ^{199}Hg line-center frequency versus lattice depth for four lattice wavelengths, measured using the $\Delta\nu_L$∼150 Hz spectra. The frequency (ordinate axis) is offset by $\nu_{\rm Hg} = 1\,128\,575\,290\,808\,162.0$ Hz. The lines of best fit roughly intersect at a common frequency at zero optical power, as is expected. The line slopes determine the differential light shift, and the wavelength at which the differential light shift is zero determines the magic wavelength λ_m. These measurements alone produced an improved estimate of $\lambda_m = 362.569 \pm 0.007$ nm, which was a necessary step leading to the detection of the ultranarrow transition (with $\Delta\nu_L$∼15 Hz). Subsequent light shift measurements with the ultranarrow spectra, such as those shown in Fig. 8(a), produce a higher-resolution measurement of λ_m. Below $16E_R$ the SNR deteriorates quickly, hence the lack of data here. Combining all available data, the magic wavelength is determined to be $\lambda_m = 362.5697 \pm 0.0011$ nm [19], where the final uncertainty

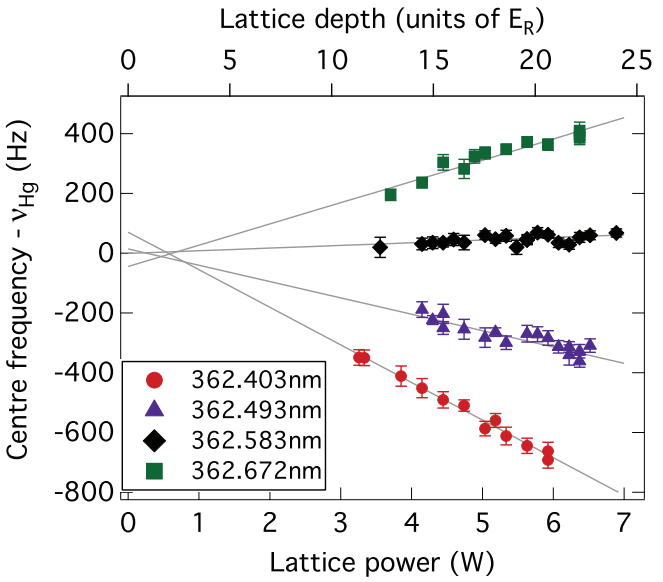

FIG. 7. (Color online) ^{199}Hg clock transition frequency versus power for four separate wavelengths. Measurements were recorded with $\Delta\nu_L \sim 150$ Hz spectra.

is dominated by that of the wavemeter. This λ_m measurement is supported by the Lorentzian linewidth versus lattice wavelength measurements shown in Fig. 8(b). There is a definite broadening of the line as the lattice wavelength is shifted away from the magic wavelength. The uncertainties on the linewidths tend to increase with detuning away from λ_m as the SNR falls.

V. FREQUENCY MEASUREMENTS

To ensure accuracy of the line-center frequencies, the spectra are recorded simultaneously with frequency comb measurements of the ultrastable laser (USL) light. The experimental setup for the link between the 265.6-nm clock probe signal and the 1062.6-nm light sent to the comb is illustrated in Fig. 9. Optical fiber links exist between the USL and the main Hg table (with polarization-preserving fiber), as well as between the USL and the frequency comb (with standard single-mode fiber). The environmental noise imposed on the fibers is actively canceled through the use of a double-passed

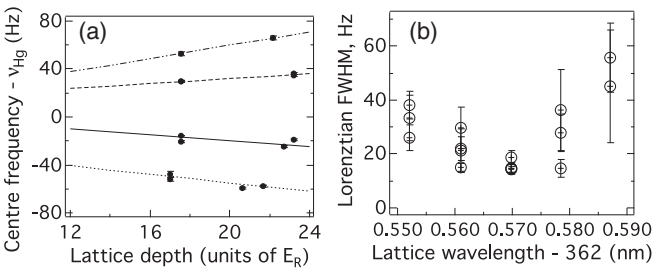

FIG. 8. (a) The ^{199}Hg $^1S_0 - {}^3P_0$ transition frequency versus lattice depth for four wavelengths based on $\Delta\nu_L \sim 15$ Hz spectra. From top to bottom: $\lambda_L = 362.587$ nm, 362.579 nm, 362.561 nm and 362.552 nm. (b) The ^{199}Hg $^1S_0 - {}^3P_0$ transition linewidth versus lattice wavelength.

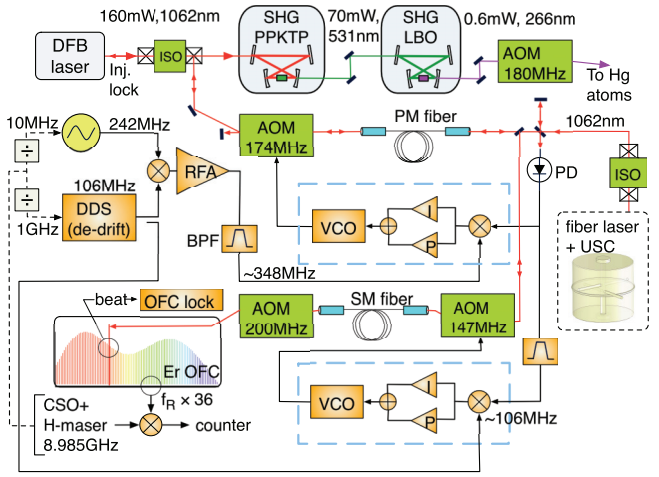

FIG. 9. (Color online) Schematic illustrating the optical links between the ultrastable laser, the Hg atoms, and one of the frequency combs used. Also shown are the fiber noise-cancellation schemes, which are used concurrently with frequency drift cancellation of the ultrastable laser light through the use of the direct digital synthesizer (DDS). The drift cancellation is applied to the 1062.6-nm light sent to the distributed feedback diode laser (DFB) and to the frequency comb in equal measure. AOM, acousto-optic modulator; BPF, bandpass filter; I, integral gain; ISO, isolator; OFC, optical frequency comb; P, proportional gain; PD, photodiode; PM, polarizing maintaining; RFA, radio-frequency amplifier; SHG, second-harmonic generation; SM, single mode; USC, ultrastable cavity; VCO, voltage-controlled oscillator.

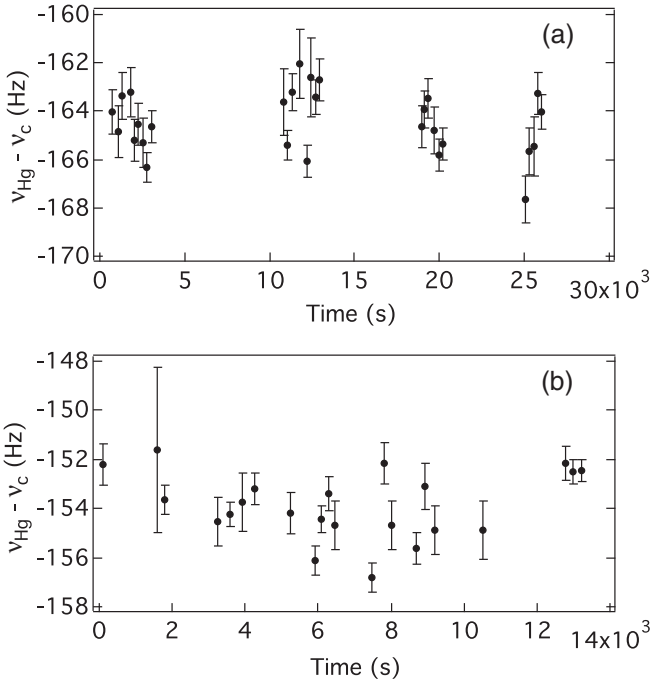

FIG. 10. (a) and (b) ^{199}Hg $^1S_0 - {}^3P_0$ frequency measurements recorded over two separate days based on line-profile measurements. The measurements are made with respect to a calibrated cryogenic sapphire oscillator + H-maser signal via a frequency comb and $\lambda_L =$ 362.5697 nm. MJD = 55809 and 55889 for (a) and (b), respectively.

acousto-optic modulator (AOM). These AOMs also provide a means of subtracting the remaining frequency drift of the USL. With the aid of a (direct) digital synthesizer (DDS), both the light received by the ^{199}Hg atoms and the IR light reaching the frequency comb have the drift of the USL removed so that the residual drift rate is below 1 mHz s^{-1} (in the IR). There is a second frequency comb, not shown in Fig. 9, where the USL frequency drift cancellation is implemented in a similar manner. One frequency comb is a mode-locked Er:fiber-laser-based comb, and the other is a mode-locked Ti:sapphire-laser-based comb. The use of two combs helped to confirm the accuracy of the measurements. For about 90% of the ^{199}Hg spectra recorded, the fiber-laser-based comb was employed, and in the remaining 10% both combs were used.

Line-center frequency measurements for the ^{199}Hg clock transition recorded over the period of 2 days [modified Julian day (MJD) = 55809 and 55889, respectively] are shown in Figs. 10(a) and 10(b). During each sweep of the clock transition the laser frequency was stepped at least 40 times in 2-Hz intervals. One scan of the clock transition [e.g., Fig. 5(a)] consisted of at least four consecutive sweeps and required, on average, 220 s of acquisition time. Each scan produces a separate data point in Fig. 10. The uncertainty for each measurement is determined from the line fitting, where a Lorentzian line shape is applied to the spectra. Each measurement is initially made with respect to the cryogenic sapphire oscillator (CSO) + H-maser frequency combination that produces the 8.895-GHz microwave reference indicated in Fig. 9 [40] (since this signal is more easily distributed throughout the various laboratories). The weighted mean and standard deviation of these data are used to establish a frequency measurement for the respective MJDs. For example, for Figs. 10(a) and 10(b) they are $\nu_{Hg} = \nu_C - 164.67 \pm 1.30$ Hz and $\nu_{Hg} = \nu_C - 153.86 \pm 1.35$ Hz, respectively, where $\nu_C =$ 1 128 575 290 808 400 Hz is the frequency of the ^{199}Hg $^1S_0 - {}^3P_0$ transition measured using Doppler-free spectroscopy on laser-cooled atoms [41]. This acted as a convenient reference value until the more accurate frequency was determined.

Over the course of 3 months $n = 30$ of such measurements were carried out (corresponding to 30 separate days). This is shown in Fig. 11(a), where between 10 and 30 line-profile measurements were made per day. Where there was a small change in the lattice light wavelength between MJDs, the frequencies were corrected to correspond to that for $\lambda_m =$ 362.5697 nm using the light shift slope of $-6 \times 10^{-17} E_R^{-1}$ GHz^{-1}. The mean values from Figs. 10(a) and 10(b) are included in the data of Fig. 11(a). Measurements between the CSO + H-maser ensemble and the LNE-SYRTE Cs primary frequency standard were made continually through the course of the Hg measurements. Figure 11(b) shows the frequency difference between the CSO + H maser and the Cs PFS translated to the carrier frequency at ν_{Hg}.

By accounting for the drift of the CSO + H-maser frequency, we find the ^{199}Hg line-center frequency measurements with respect to the PFS. These are summarized in Fig. 6 of Ref. [19]. A line-of-best fit with zero slope produces a weighted mean of 0.29 Hz (or 2.5×10^{-16} in fractional frequency) with a goodness-of-fit parameter equal to 0.91 (equal to $\Gamma[(n-1)/2, \chi^2/2]$, where $\Gamma(s,x)$ is the regularized

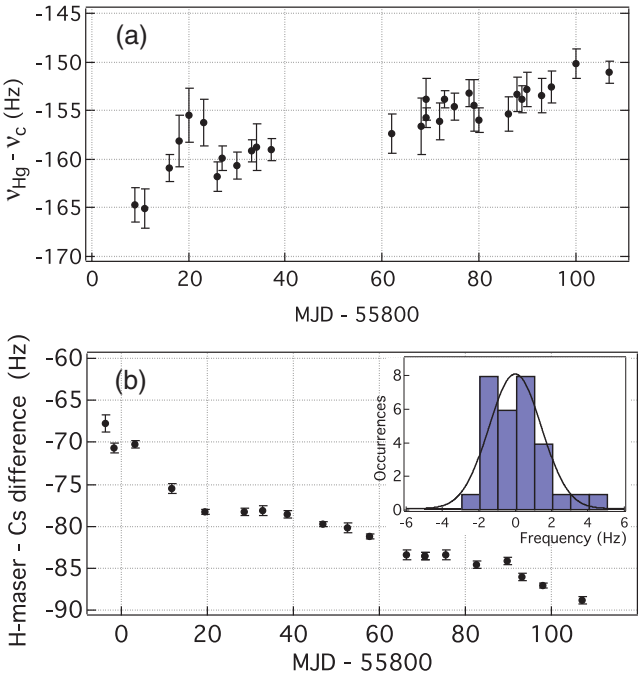

FIG. 11. (Color online) (a) Frequency measurements of the ^{199}Hg clock transition with respect to the CSO + H-maser reference. (b) CSO + H-maser comparison with the LNE-SYRTE primary frequency standard, where the fractional difference is multiplied by the ^{199}Hg carrier frequency of 1.1286 PHz. The inset shows the histogram of the ^{199}Hg absolute frequency measurements with respect to the LNE-SYRTE primary frequency standard. MJD, modified Julian Day.

lower incomplete Gamma function and $\chi^2/(n-1) = 0.64$; hence the Birge ratio = 0.80). The mean value of these data was used to establish a new frequency for the ^{199}Hg $^1S_0 - {}^3P_0$ transition, namely, $\nu_{Hg} = 1\ 128\ 575\ 290\ 808\ 162 \pm 6.4$ Hz (dominated by systematic uncertainties) [19]. These absolute frequency measurements are binned in 1-Hz intervals and displayed as a histogram in the inset of Fig. 11(b). The 1σ value for the fitted normal distribution is 1.56 Hz. Dividing by $\sqrt{n}$ again gives a statistical uncertainty of 0.29 Hz, demonstrating consistency between the statistical methods. This very small uncertainty bodes well for the ^{199}Hg $^1S_0 - {}^3P_0$ transition as a frequency reference. We note that the mean fractional frequency drift between the CSO + H maser and PFS is -1.5×10^{-16} per day over the course of these measurements.

VI. CONCLUSIONS

We have described the $(6s^2)\,{}^1S_0 - (6s6p)^3P_0$ spectroscopy of ^{199}Hg atoms in a one-dimensional lattice trap of depth $\lesssim 25 E_R$ at the nonperturbing magic wavelength. A consistent $\sim$15 Hz FWHM spectral line has been used to assess the $^1S_0 - {}^3P_0$ transition's reproducibility. We have demonstrated a statistical fractional frequency uncertainty of 2.5×10^{-16} for an ultraviolet atomic transition measured against the LNE-SYRTE primary frequency standard, where the data were recorded over a 3-month period. These results were obtained despite some anomalous behavior where the $\sim$15-Hz-wide clock signal is found located at the center of a broader spectral feature (FWHM $\sim$ 150 Hz). We postulate that the broader spectral feature is due to atoms escaping from the trap during the probe time of the clock transition. In future, a deeper trap will be used as a means of testing this hypothesis. The results here show the potential of the Hg clock transition as a high-accuracy frequency reference, as one may expect the overall fractional frequency uncertainty to reduce to near that of the statistical uncertainty when further analyses of systematic shifts are undertaken.

ACKNOWLEDGMENTS

We express thanks to M. Lours and F. Cornu for their valuable assistance. SYRTE is Unité Mixte de Recherche 8630 of the Centre National de la Recherche Scientifique (CNRS) and is associated with the Université Pierre et Marie Curie (UPMC). This work is partly funded by the Institut Francilien de Recherche sur les Atomes Froids (IFRAF) and by the Centre National d' Études Spatiales (CNES).

[1] P. Gill, Philos. Trans. R. Soc. A **369**, 4109 (2011).
[2] T. E. Parker, Rev. Sci. Instrum. **83**, 021102 (2012).
[3] X. Calmet and H. Fritzsch, Phys. Lett. B **540**, 173 (2002).
[4] S. G. Karshenboim and E. Peik, Eur. Phys. J. Spec. Top. **163**, 1 (2008).
[5] T. Rosenband, D. B. Hume, P. O. Schmidt, C. W. Chou, A. Brusch, L. Lorini, W. H. Oskay, R. E. Drullinger, T. M. Fortier, J. E. Stalnaker, S. A. Diddams, W. C. Swann, N. R. Newbury, W. M. Itano, D. J. Wineland, and J. C. Bergquist, Science **319**, 1808 (2008).
[6] S. Blatt, A. D. Ludlow, G. K. Campbell, J. W. Thomsen, T. Zelevinsky, M. M. Boyd, J. Ye, X. Baillard, M. Fouche, R. Le Targat, A. Brusch, P. Lemonde, M. Takamoto, F. L. Hong, H. Katori, and V. V. Flambaum, Phys. Rev. Lett. **100**, 140801 (2008).
[7] J. Guéna, M. Abgrall, D. Rovera, P. Rosenbusch, M. E. Tobar, Ph. Laurent, A. Clairon, and S. Bize, Phys. Rev. Lett. **109**, 080801 (2012).
[8] T. M. Fortier, N. Ashby, J. C. Bergquist, M. J. Delaney, S. A. Diddams, T. P. Heavner, L. Hollberg, W. M. Itano, S. R. Jefferts, K. Kim, F. Levi, L. Lorini, W. H. Oskay, T. E. Parker, J. Shirley, and J. E. Stalnaker, Phys. Rev. Lett. **98**, 070801 (2007).
[9] F.-L. Hong, M. Musha, M. Takamoto, H. Inaba, S. Yanagimachi, A. Takamizawa, K. Watabe, T. Ikegami, M. Imae, Y. Fujii, M. Amemiya, K. Nakagawa, K. Ueda, and H. Katori, Opt. Lett. **34**, 692 (2009).
[10] O. Lopez, A. Haboucha, F. Kefelian, Haifeng Jiang, B. Chanteau, V. Roncin, C. Chardonnet, A. Amy-Klein, and G. Santarelli, Opt. Express **18**, 16849 (2010).
[11] A. Yamaguchi, M. Fujieda, M. Kumagai, H. Hachisu, S. Nagano, Ying Li, T. Ido, T. Takano, M. Takamoto, and H. Katori, Appl. Phys. Express **4**, 082203 (2011).
[12] K. Predehl, G. Grosche, S. M. F. Raupach, S. Droste, O. Terra, J. Alnis, Th. Legero, T. W. Hänsch, Th. Udem, R. Holzwarth, and H. Schnatz, Science **336**, 441 (2012).

[13] L. Cacciapuoti and C. Salomon, Eur. Phys. J. Spec. Top. **172**, 57 (2009).
[14] S. Schiller *et al.*, Exp. Astron. **23**, 573 (2009).
[15] L. Duchayne, F. Mercier, and P. Wolf, Astron. Astrophys. **504**, 653 (2009).
[16] J. Müller, M. Soffel, and S. A. Klioner, J. Geod. **82**, 133 (2008).
[17] R. Bondarescu, M. Bondarescu, G. Hetenyi, L. Boschi, P. Jetzer, and J. Balakrishna, Geophys. J. Int. **191**, 78 (2012).
[18] H. Hachisu, K. Miyagishi, S. G. Porsev, A. Derevianko, V. D. Ovsiannikov, V. G. Pal'chikov, M. Takamoto, and H. Katori, Phys. Rev. Lett. **100**, 053001 (2008).
[19] J. J. McFerran, L. Yi, S. Mejri, S. Di Manno, W. Zhang, J. Guéna, Y. Le Coq, and S. Bize, Phys. Rev. Lett. **108**, 183004 (2012).
[20] J. J. McFerran, D. V. Magalhaes, C. Mandache, J. Millo, W. Zhang, Y. Le Coq, G. Santarelli, and S. Bize, Opt. Lett. **37**, 3477 (2012).
[21] A. D. Ludlow, T. Zelevinsky, G. K. Campbell, S. Blatt, M. M. Boyd, M. H. G. de Miranda, M. J. Martin, L. W. Thomsen, S. M. Foreman, Jun Ye, H. T. M. Fortier, E. Stalnaker, S. A. Diddams, Y. Le Coq, Z. W. Barber, N. Poli, H. N. D. Lemke, K. M. Beck, and C. W. Oates, Science **319**, 1805 (2008).
[22] N. D. Lemke, A. D. Ludlow, Z. W. Barber, T. M. Fortier, S. A. Diddams, Y. Jiang, S. R. Jefferts, T. P. Heavner, T. E. Parker, and C. W. Oates, Phys. Rev. Lett. **103**, 063001 (2009).
[23] J. A. Sherman, N. D. Lemke, N. Hinkley, M. Pizzocaro, R. W. Fox, A. D. Ludlow, and C. W. Oates, Phys. Rev. Lett. **108**, 153002 (2012).
[24] T. Middelmann, S. Falke, C. Lisdat, and U. Sterr, Phys. Rev. Lett. **109**, 263004 (2012).
[25] T. E. Parker, Metrologia **47**, 1 (2010).
[26] J. Guena, M. Abgrall, D. Rovera, P. Laurent, B. Chupin, M. Lours, G. Santarelli, P. Rosenbusch, M. E. Tobar, R. Li, K. Gibble, A. Clairon, and S. Bize, IEEE Trans. Ultrason. Ferroelectr. Freq. Control **59**, 391 (2012).
[27] R. Le Targat *et al.*, Nat. Commun. **4**, 2109 (2013).
[28] N. Huntemann, M. Okhapkin, B. Lipphardt, S. Weyers, Chr. Tamm, and E. Peik, Phys. Rev. Lett. **108**, 090801 (2012).
[29] B. J. Bloom, T. L. Nicholson, J. R. Williams, S. L. Campbell, M. Bishof, X. Zhang, W. Zhang, S. L. Bromley, and J. Ye, Nature (London) **506**, 71 (2014).
[30] J. Millo, D. V. Magalhães, C. Mandache, Y. Le Coq, E. M. L. English, P. G. Westergaard, J. Lodewyck, S. Bize, P. Lemonde, and G. Santarelli, Phys. Rev. A **79**, 053829 (2009).
[31] S. T. Dawkins, R. Chicireanu, M. Petersen, J. Millo, D. V. Magalhaes, C. Mandache, Y. Le Coq, and S. Bize, Appl. Phys. B **99**, 41 (2009).
[32] Y. Asakawa, H. Kumagai, K. Midorikawa, and M. Obara, Opt. Commun. **217**, 311 (2003).
[33] S. Mejri, J. J. McFerran, L. Yi, Y. Le Coq, and S. Bize, Phys. Rev. A **84**, 032507 (2011).
[34] K. M. O'Hara, S. R. Granade, M. E. Gehm, T. A. Savard, S. Bali, C. Freed, and J. E. Thomas, Phys. Rev. Lett. **82**, 4204 (1999).
[35] T. A. Savard, K. M. O'Hara, and J. E. Thomas, Phys. Rev. A **56**, R1095(R) (1997).
[36] However, the parametric heating model used is simplistic, ignoring, for example, highly excited trap states and gravity.
[37] L. Yi, S. Mejri, J. J. McFerran, Y. Le Coq, and S. Bize, Phys. Rev. Lett. **106**, 073005 (2011).
[38] R. Le Targat, Ph.D. thesis, Ecole nationale supérieure des telecommunications, 2007, p. 125; http://tel.archives-ouvertes.fr/tel-00170038/fr/.
[39] A.-D. Ludlow, M. M. Boyd, T. Zelevinsky, S. M. Foreman, S. Blatt, M. Notcutt, T. Ido, and J. Ye, Phys. Rev. Lett. **96**, 033003 (2006).
[40] D. Chambon, S. Bize, M. Lours, F. Narbonneau, H. Marion, A. Clairon, G. Santarelli, A. Luiten, and M. Tobar, Rev. Sci. Instrum. **76**, 094704 (2005).
[41] M. Petersen, R. Chicireanu, S. T. Dawkins, D. V. Magalhaes, C. Mandache, Y. Le Coq, A. Clairon, and S. Bize, Phys. Rev. Lett. **101**, 183004 (2008).